IEEE Journal of Microwaves

Received 3 November 2021; revised 5 January 2022; accepted 19 January 2022. Date of publication 9 February 2022; date of current version 7 April 2022.

Digital Object Identifier 10.1109/JMW.2022.3145906

Miniaturized Dual-Band Dual-Mode TM-Mode Dielectric Filter in Planar Configuration

ABDULRAHMAN WIDAA (Graduate Student Member, IEEE), AND MICHAEL HÖFT (Senior Member, IEEE)

(Regular Paper)

Chair of Microwave Engineering, Kiel University, 24143 Kiel, Germany

CORRESPONDING AUTHOR: Abdulrahman Widaa (e-mail: aw@tf.uni-kiel.de).

This work was supported in part by the European Union's Horizon 2020 Research and Innovation Programme under the Marie Skłodowska-Curie Grant agreement 811232-H2020-MSCA-ITN-2018 and in part by the DFG Open Access Publication Funding Programme of Kiel University.

ABSTRACT This paper reports a new class of compact inline dual-band bandpass filters using TM-mode dielectric resonators in planar configuration. Thanks to the employment of the dielectric-loaded TM-mode waveguide configuration and the dual-mode TM_{120} and TM_{210} resonances, substantial size miniaturization and volume saving (>70%) can be obtained in comparison with conventional waveguide technology. Additionally, the planar topology of the presented concept offers highly desirable advantages for industry and mass production including the ease of manufacturing, assembly, and tuning. Furthermore, the resonating doublets and the nonresonating TM_{110} mode are effectively utilized to introduce and control both inter-band and outer-band transmission zeros, advantageously increasing the isolation between the two passbands and enhancing the outer-band rejection regions. The general design procedure of the proposed filter is discussed in detail. A three-pole C-band dual-band dual-mode TM-mode dielectric filter is designed, implemented, and measured to validate the proposed configuration.

INDEX TERMS Bandpass filter, dual-band, dual-mode, dielectric resonator, TM-mode.

I. INTRODUCTION

The Current rapid development of multi-channel/multi-standard RF and satellite communications have urged the demand for more efficient, compact, and lightweight multi-band payloads and subsequent filtering units. Often, those essential requirements cannot be effectively fulfilled using the conventional single-band filter structures, and more efficient multi-band designs are needed [1]. Accordingly, various dual-band bandpass filters were introduced in the literature using different technologies and configurations [2]—[12]. Whereas the majority of the presented dual-band bandpass filters are developed using compact planar microstrip and SIW structures as presented in [2] and [3], they are not favorable in satellite and high-performance communications due to the high losses and limited power handling capabilities. Therefore, high-Q and high-power compatible waveguide cavities have gained more interest in the implementation of dual-band BPFs [4]—[6]. For example, [4] introduced a new class of waveguide dual-band bandpass filters in an in-line configuration using dual-mode TE_{101}/TE_{011} modes for size reduction. However, a special milling machining is required to realize such structures, and cross-couplings cannot be introduced to generate additional transmission zeros (TZs). Folded side-coupled dual-band dual-mode TE_{11m} mode elliptical cavity filters were presented in [5] to facilitate the cross-coupling and TZs' creation. Nevertheless, the proposed filters suffer from many unwanted spurious resonances and inflexibility in controlling the transmission zeros' positions. In addition to the aforementioned limitations of empty-cavity waveguide dual-band filters, more size reduction and lighter weight are still required. This motivated the introduction of more compact dual-band coaxial and dielectric-loaded waveguide filters [7]—[12]. Work performed by [9] presented a 3rd-order dual-band filter using an open-circuited-stub-loaded quarter-wavelength coaxial resonator. The bandpass filter operates at 0.9 GHz and 2 GHz bands with a single uncontrolled inter-band transmission zero. A third-order dual-band filter was introduced in [10] using dielectric resonators to offer a more compact size and higher Q_u than the other configurations. However, specially customized dielectric resonators and

assembly processes are needed to implement the filter. Besides, the filter suffers from close spurious modes and limited selectivity due to the difficulty in the introduction and control of transmission zeros. All of these drawbacks limit the extension of the proposed dual-band DR filter to higher orders and also to use in industry.

TM mode dielectric resonators are particularly favorable in filter applications due to their substantial size miniaturization, mechanical stability, high Q_u, and wider spurious-free band [13]. To take the advantage of all these desirable features with considering the limitations of the aforementioned dual-band filter structures, the authors in [11] introduced a new highly compact dual-band dual-mode TM mode dielectric filter with more than 90% reduced volume than the conventional waveguide structures. The dual-band response is realized through properly modifying the transverse doublet structure. Additionally, the coupling scheme is adjusted to move at least one transmission zero between the two passbands to enhance the inter-band isolation. However, this transversal configuration has many drawbacks including difficult tuning, sensitivity to TZs locations, and precise selection of iris locations. Additionally, since the filter is built out of separated transversal blocks, this leads to more assembly time and cost, and can also increase the related losses. Therefore, alternative dual-band TM-mode dielectric-loaded configurations are required to benefit from the TM mode DR advantages and overcome the challenges of the transversal topology.

A new miniaturized C-band dual-band dual-mode TM-mode dielectric filter is presented in this paper. The filter is designed in planar configuration for the purposes of easy tuning, manufacturing, and assembly. Additionally, enhanced inter-band isolation and outer-band rejection are realized through flexibly positioned transmission zeros. The following sections discuss the design procedure of the proposed topology and report the measured results of a three-pole dual-band dual-mode TM-mode dielectric resonator filter.

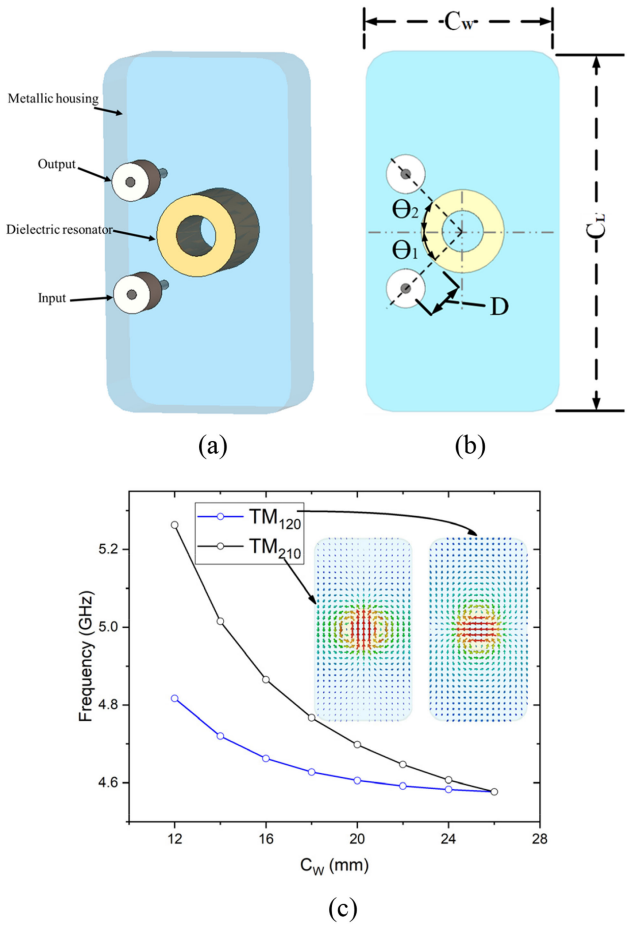

FIGURE 1. Dual-band TM mode DR cavity. (a) Perspective view. (b) Top view. Both modes TM_{120}, TM_{210} are excited equally through input probe with angle $\theta_1 = 45^o$ and output probe with angle $\theta_2 = -45°$. (c) f_{TM120}, f_{TM210} change in relation to the change in the cavity width (C_W) while the cavity length is kept unchanged (C_L = 26 mm). The TM mode dielectric resonator has outer diameter D = 8 mm, inner diameter d = 4 mm, height = 6 mm, and dielectric constant $\varepsilon_r = 45$.

II. CONCEPT AND DESIGN

A. DUAL-RESPONSE DUAL-MODE TM-MODE DIELECTRIC RESONATOR

The basic doublet block was introduced earlier in [14] and employed to design a dual-mode dielectric filter using TE mode dielectric resonators in [15]. Similarly, dual-mode TM-mode DR configurations were introduced in planar topology for miniaturized single-band fixed and tunable filters applications [16], [17]. For instance, in [17], a dual-mode filter is designed using the two orthogonal degenerate modes TM_{120} and TM_{210} in a single resonator structure. The resonant frequencies of the orthogonal modes are adjusted primarily through the cavity length (C_L) and width (C_W) where each mode is mainly propagating and more sensitive in a corresponding dimension. Herein, the cavity length and width are set equal in order to obtain the desired dual-mode passband ($C_L \approx C_W$). Alternatively, the dual-mode configuration can be altered to a dual-passband response by shifting any of the degenerate resonant frequencies away from the other one as depicted in Fig. 1. This is basically done by changing the respective dimension of any of the resonant modes ($C_L \neq C_W$). As can be seen in Fig. 1(c), both TM_{120} and TM_{210} resonate at the same central frequency (4.58 GHz) when $C_L = C_W = 26$ mm, while f_{TM210} increases and moves away from f_{TM120} with the reduction of the cavity width creating a dual-band response. The separation of the two passbands is proportionally related to the ratio between the cavity length and width (C_L/C_W). Similar to conventional doublet configurations [15], the input and output feeding probes are rotated to excite both modes with angles $\theta_1 = 45°$and $\theta_2 = -45°$, respectively. If the rotation equals to 45°, then the IO probes are coupled to both orthogonal TM_{120} and TM_{210} modes equally. If θ is less than 45°, then the IO probes are more coupled to TM_{210} while in contrary, they'll be more coupled to TM_{120} when θ is larger than 45°. θ_1 and θ_2 are related to the coupling coefficients

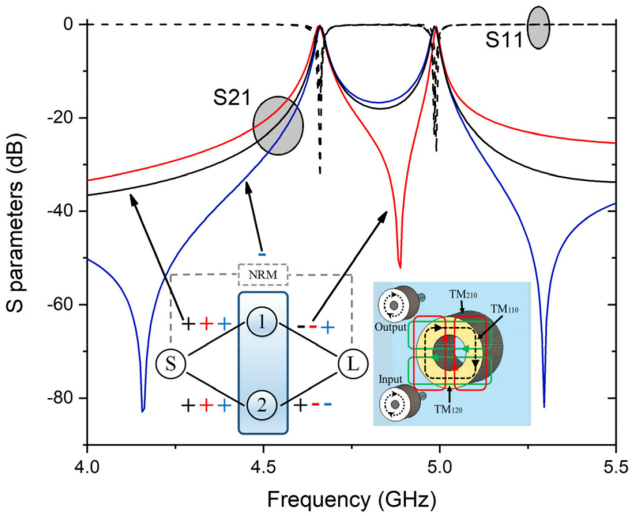

FIGURE 2. S-parameter responses of 3 different dual-band configurations and their corresponding coupling routes (black, red, blue) realized by proper excitation and orientation of the IO feedings. Dual-band response is obtained through $C_W \neq C_L$ ($f_{TM120} = 4.66$ GHz, $f_{TM210} = 4.98$ GHz). Blackline: Chebyshev responses ($M_{S2} = M_{S1}$, $M_{1L} = -M_{S1}$, $M_{2L} = M_{S2}$, $M_{SL} = 0$). Redline: inter-band TZ is introduced (sign change of M_{2L} causing a phase reversal at the output with respect to the input). Blueline: 2 TZs are introduced by the mean of the nonresonating TM_{110} mode bypass source-load coupling (NRM) ($M_{SL} < 0$). The TM mode dielectric resonator has outer diameter D = 8 mm, inner diameter d = 4 mm, height = 6 mm, and dielectric constant $\varepsilon_r = 45$. $C_W = 14$ mm, $C_L = 26$ mm.

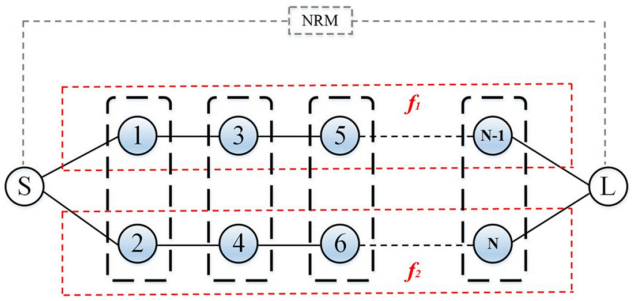

FIGURE 3. Generalized coupling scheme of the proposed dual-band dual-mode TM mode DR filters. N corresponds to the filters' orders. Each orthogonal degenerate mode creates an individual channel (f_1, f_2). In some cases, the nonresonating TM_{110} mode (NRM) is excited and creates a S-L coupling path introducing outer-band transmission zeros.

using:

$$\tan(\theta_1) = \frac{M_{S1}}{M_{S2}}, \quad \tan(\theta_2) = \frac{M_{1L}}{M_{2L}} \tag{1}$$

The angular distance between the dielectric resonator and the IO probes (D) controls the coupling strength to both modes. Fig. 2 demonstrates a dual-response cavity using a dual-mode TM-mode dielectric resonator with three different coupling routes and S parameter responses. The H-fields of the resonating TM_{120}, TM_{210}, and nonresonating TM_{110} modes are also included. The cavity length is set larger than the width to move f_{TM210} away from f_{TM120}, therefore, creating a dual-band response at 4.98 GHz and 4.66 GHz, respectively. Based on (1), the input probe is positioned at an angle $\theta_1 = 45°$ ($M_{S2} = M_{S1}$), and the output pin is rotated to an angle $\theta_2 = -45°$ ($M_{2L} = -M_{1L}$). The first path S-1-L corresponds to the lower channel (f_{TM120}) and the second route S-2-L represents the upper band (f_{TM210}). The blackline represents the basic dual-response configuration with Chebyshev characteristics ($M_{S2} = M_{S1}$, $M_{1L} = -M_{S1}$, $M_{2L} = M_{S2}$, $M_{SL} = 0$). Also, both inter-band and outer-band TZs can be easily introduced and flexibly controlled which provides high isolation between the two bands and also improves the out-of-band rejection level. The appearance of an inter-band transmission zero in the second case (redline) is due to phase reversal of the orthogonal modes at the output port with respect to the input side ($M_{S2} = M_{S1}$, $M_{1L} = -M_{S1}$, $M_{2L} = -M_{S2}$, and $M_{SL} = 0$). This is realized by rotating the output probe to an angle $\theta_2 = -135°$ to change the sign of M_{2L}. While in the third case (blueline), the bypass coupling caused by the nonresonating mode (NRM) TM_{110} mode creates a pair of outer-band transmission zeros ($M_{S2} = M_{S1}$, $M_{1L} = M_{S1}$, $M_{2L} = -M_{S2}$, $M_{SL} < 0$) [11], [14]. In this case, the output pin is rotated to an angle $\theta_2 = -225°$. All of these interesting capabilities of the proposed concept can be effectively applied to filter's configurations and will be discussed in the following sub-section.

B. DUAL-BAND DUAL-MODE TM-MODE DIELECTRIC FILTERS

The generalized coupling mechanism of the proposed miniaturized dual-band dual-mode TM-mode DR filters is depicted in Fig. 3. It is comprised of two coupling paths that are composed of directly coupled doublet blocks. Each doublet block exhibits two orthogonally resonating modes (TM_{120}, TM_{210}) at two different frequencies which create a dual-passband response. Also, in particular configurations, the nonresonating fundamental TM_{110} mode is employed to create a bypass source-load coupling path that introduces additional transmission zeros [18]. The general design procedure begins with the synthesis and extraction of the corresponding coupling scheme and parameters of each passband individually which has been then optimized and applied to the overall dual-band response and any additional transmission zeros [19]. The coupling matrices in this paper are extracted following simple steps:

1) A good start point is by using the standard synthesis method [20] to extract the coupling matrix of every single passband individually (f_1, ABW_1), (f_2, ABW_2) with an order of N/2 for each band.
2) Normalize both channels to a single-band N-order filter using the pre-synthesized values from the first step. The 1, 2, 3, ….N/2 resonators from the first and second single-band filters represent 1, 3, 5, …..N-1 path and 2, 4, 6, ….N channel, respectively, and constitute the initial

coupling coefficients of the overall matrix (M_{i,j_0}). The chosen channel has a centre frequency $f_0 = (f_1+f_2)/2$, and an absolute bandwidth $ABW_0 = ABW_1$. Note that f_0, ABW_0, and normalized coupling coefficients can also be chosen arbitrarily [19]. The mutual and self-couplings are calculated using:

$$M_{i,i} = -\frac{f_0}{ABW_0} \times \left(\frac{f_1}{f_0} - \frac{f_0}{f_1}\right), \quad i = 1, 3, \ldots\ldots, N-1 \tag{2a}$$

$$M_{i+1,i+1} = -\frac{f_0}{ABW_0} \times \left(\frac{f_2}{f_0} - \frac{f_0}{f_2}\right), \quad i = 1, 3, \ldots\ldots, N-1 \tag{2b}$$

$$M_{i,j} = M_{i,j\_0} \times \frac{f_0}{f_1} \times \frac{ABW_1}{ABW_0}, \quad i = 1, 3, \ldots\ldots, N-3,\ j = i+2 \tag{3a}$$

$$M_{i+1,j+1} = M_{i+1,j+1\_0} \times \frac{f_0}{f_2} \times \frac{ABW_2}{ABW_0}, \quad i = 1, 3, \ldots\ldots, N-3,\ j = i+2 \tag{3b}$$

$$M_{S1} = \sqrt{\frac{f_0}{Q_{ext\_1} \times ABW_0}}, \quad M_{S2} = \sqrt{\frac{f_0}{Q_{ext\_2} \times ABW_0}} \tag{4}$$

where Q_{ext_1} and Q_{ext_2} are the calculated external quality factors from the coupling matrices of the single-band filters from the first step. Next, the required physical coupling coefficients (K) and external quality factors (Q_{ext}) for the lower passband (f_1) and higher passband (f_2) are calculated using the corresponding f_0 and bandwidth (ABW_0) as follows:

$$K_{i,j} = \frac{ABW_0 \times M_{i,j}}{f_0}, \quad i = 1, 3, \ldots\ldots, N-3,\ j = i+2 \tag{5a}$$

$$K_{i+1,j+1} = \frac{ABW_0 \times M_{i+1,j+1}}{f_0}, \quad i = 1, 3, \ldots\ldots, N-3,\ j = i+2 \tag{5b}$$

$$Q_{ext\_1} = \frac{f_0}{ABW_0 \times M_{S1}^2}, \quad Q_{ext\_2} = \frac{f_0}{ABW_0 \times M_{S2}^2} \tag{6}$$

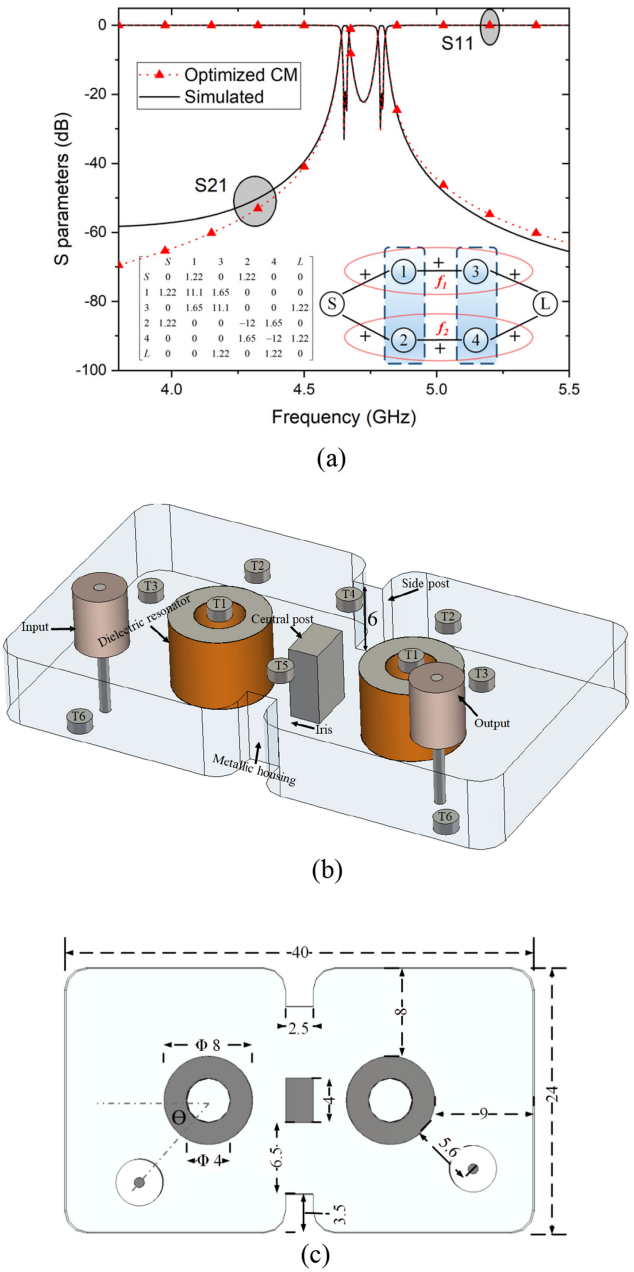

FIGURE 4. Second-order dual-band dual-mode TM-mode DR filter in aligned IO configuration. (a) Coupling scheme, optimized coupling matrix (redline), and simulted S-parameters (blackline): no inter-band transmission zero ($M_{3L} = M_{S1}$, $M_{4L} = M_{S2}$), and no outer-band transmission zero ($M_{SL} = 0$). (b) Perspective view. (c) Top view. All dimensions in mm unit.

Afterward, the dual-band bandpass filter is realized using the presented dual-mode TM mode dielectric resonators. Figs. 4 to 13 show two design examples of second and third-order dual-band TM mode DR filters based on the proposed planar topology, respectively. SMA connectors are used for the I/O feeding and a compact TM mode DR (outer diameter = 8 mm, inner diameter = 4 mm, height = 6 mm) is also employed with a high dielectric constant of 45 to provide more volume reduction. Considering the fields' coupling nature of the two orthogonal modes, the required dual-band response cannot be obtained with conventional coupling irises configurations because they cannot provide the required isolation between the two modes. Therefore, inductive rectangular posts are effectively employed to obtain the required inter-resonator

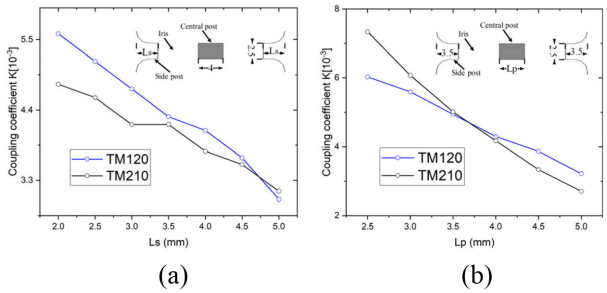

FIGURE 5. Relationship between the physical coupling coefficients of TM_{120} and TM_{210} modes and (a) side posts length Ls, and (b) central post length Lp.

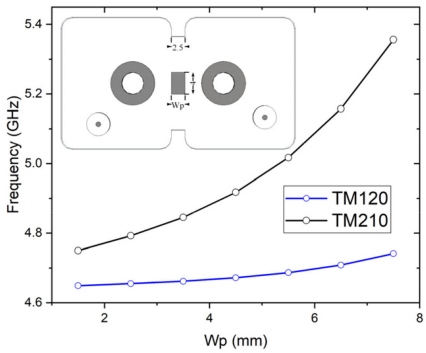

FIGURE 6. Dependence of f_{TM120} and f_{TM210} on the central post width Wp.

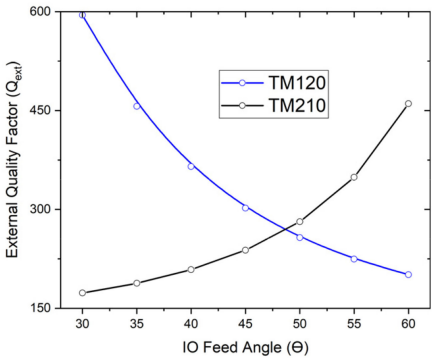

FIGURE 7. External quality factors of TM_{120}, and TM_{210} modes in relation to the rotation of the IO probe.

couplings and provide bands' isolation and separation. The IO feedings are rotated to excite both orthogonal modes at the same time as discussed earlier. Fig. 4 demonstrates a 2nd-order dual-band filter of the proposed structure operates at 4.65 GHz and 4.79 GHz with a narrow bandwidth of 12 MHz at both passbands. The coupling topology and optimized matrix are provided in Fig. 4(a) following the aforementioned procedure. The simulated S-parameter responses are also included in Fig. 4(a) with excellent agreement with the required specifications. The simulated Q_u for the first passband is 3440 and 3330 for the higher band. Fig. 4(b) shows the realized dual-band BPF using dual-mode TM-mode DR in planar configurations. The TM_{120} mode constructs the lower passband (f_1) while the higher channel (f_2) is formed by the orthogonal TM_{210} mode. As shown earlier, the separation between the resonant frequencies of the two modes is mainly controlled by the cavity length/width ratio. In this example, the two channels are closely-spaced with 140 MHz separation. The required inter-resonator couplings of both passbands (K_{13}, K_{24}) are realized using common inductive irises with side and central inductive posts. The relation between the coupling coefficients (K) of TM_{120} (K_{13}), TM_{210} (K_{24}) channels and the central and side posts is depicted in Fig. 5. The inter-resonator coupling of the first passband is more controlled by the side posts (Ls) since the TM_{120} mode resonates mainly in sides and it is less distributed in the centre of the cavity (see Fig. 1(c)). In contrast, the coupling bandwidth of the upper passband is more related to the central post (Lp) as the TM_{210} mode is more distributed in the centre of the cavity than the sides. Furthermore, as the central post is located close to the maximum of the TM_{210} mode, the post width (Wp) can be altered to push the TM_{210} channel further away from the TM_{120} mode passband as can be seen in Fig. 6. All these capabilities advantageously provide a more relaxed degree-of-freedom to the designers towards getting different/similar bandwidths at the two passbands with extended spacing. Tuning screws can be introduced easily and utilized effectively in this planar structure to compensate for various tolerances and retain the required response. The inter-resonator couplings of both passbands can be tuned through T4 and T5, while T1 is used to tune the resonant frequency of both bands at the same time (frequencies will move up with tuning [17]). Furthermore, T2 and T3 can be employed to tune the lower (TM_{120}) and upper (TM_{210}) bands independently (frequencies will decrease with tuning). Similarly, T6 can be added to control the IO coupling.

The desired external quality factors Q_{ext_1} (TM_{120}), Q_{ext_2} (TM_{210}) are realized using inductive probes rotated with an angle θ. The dependence of Q_{ext_1} and Q_{ext_2} on the rotation angle of the IO probe is presented in Fig. 7. As shown, Q_{ext_1} of TM_{120} increases with smaller angles whereas Q_{ext_2} of TM_{210} is decreasing, and vice versa.

The introduced dual-band filter has Chebyshev outer-band response and inter-band isolation at 22 dB level. These two aspects need to be enhanced for high-performance applications. Therefore, the introduction of inter-band and outer-band TZs is importantly needed to improve the isolation between the two channels and the outer-band selectivity. [21] presented a detailed overview of the TZs' generation in multi-path coupling structures. Similarly, [22] showed that a TZ can be created between the passbands through the proper orientation of the feeding waveguides to cause a phase reversal between the signals traveling through different paths. The same concept can be employed effectively and more flexibly in

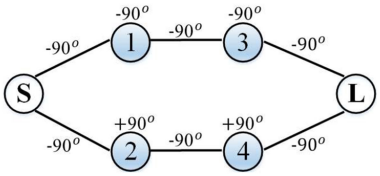

FIGURE 8. Phase shift diagram of the presented two-pole dual-band dual-mode filter in in-phase configuration (Fig. 4).

TABLE 1. Total Phase Shifts for the Two Paths of the Two-Pole Dual-Band Filters

Filter		Phase shift at the transmission zero's frequency
1st filter with no inter-band TZ	Lower passband (Resonators 1, 3)	$-90^{\circ}-90^{\circ}-90^{\circ}-90^{\circ}-90^{\circ}=\mathbf{-90^{\circ}}$
	Upper passband (Resonators 2, 4)	$-90^{\circ}+90^{\circ}-90^{\circ}+90^{\circ}-90^{\circ}=\mathbf{-90^{\circ}}$
	Result	**In-phase**
2nd filter with inter-band TZ	Lower passband (Resonators 1, 3)	$-90^{\circ}-90^{\circ}-90^{\circ}-90^{\circ}\mathbf{+90^{\circ}}=\mathbf{-270^{\circ}}$
	Upper passband (Resonators 2, 4)	$-90^{\circ}+90^{\circ}-90^{\circ}+90^{\circ}\mathbf{-90^{\circ}}=\mathbf{-90^{\circ}}$
	Result	**Out-of-phase**

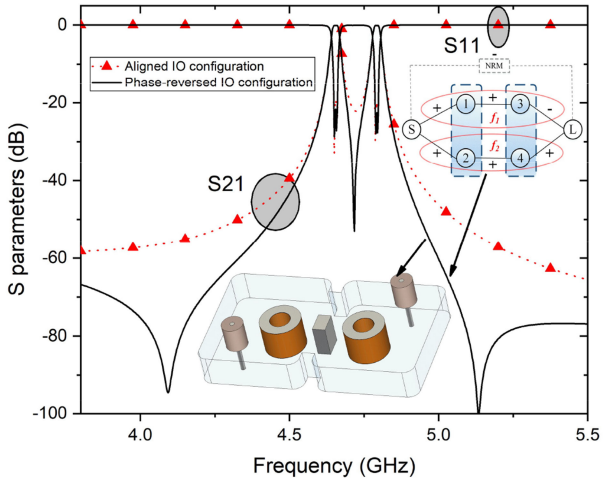

FIGURE 9. Second-order dual-band dual-mode TM-mode DR filter in phase-reversed configuration. Inter-band transmission zero is introduced ($M_{3L} = -M_{S1}$, $M_{4L} = M_{S2}$), and outer-band transmission zeros are created ($M_{SL} < 0 = -.0004$).

the proposed dual-band TM-mode DR filter configuration. In the original structure in Fig. 4, the input and output probes are in aligned configuration with the same angle ($\theta_2 = \theta_1$). The phase change diagram of the presented filter is demonstrated in Fig. 8. All couplings are inductive with reference to the corresponding coupling topology in Fig. 4. As can be seen in Table 1, the signals of both bands are in-phase to each other, hence, no inter-band transmission zero can be introduced. An inter-band TZ is generated if the output probe is rotated by 90° for phase reversal between the two modes. Fig. 9

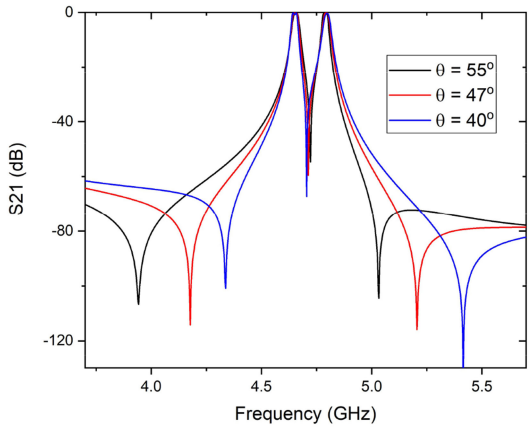

FIGURE 10. Outer-band transmission zeros relation to the IO feeding angle.

depicts the phase-reversed IO configuration of the presented filter with its corresponding coupling route and simulated S parameters. As can be seen, inter-band transmission zero is effectively generated. As the output probe is rotated by 90°, the sign of M_{3L} changes to negative causing the two channels to be coupled out-of-phase as shown in Table 1. Thus, a transmission zero is introduced between the two passbands enhancing the isolation to more than 50 dB. In addition to the creation of the inter-band transmission zero, the 90° rotation of the output probe also excites the non-resonating fundamental TM_{110} mode creating a source-load (S-L) coupling path ($M_{SL} = -0.0004$) introducing two asymmetrical transmission zeros below and above the filter passbands at 4.1 GHz and 5.1 GHz, respectively. The introduction and control process of the transmission zeros due to the nonresonating modes are well explained in [23] at transversal TM-mode structures. In principle, multiple inter-band and outer-band transmission zeros can be introduced and controlled in the proposed planar configurations. However, this is practically challenging since the IO probes will need to be rotated close to/inside the coupling irises unlike the transversal configurations [11] where the IO feedings can be rotated freely 360°. This limits the flexibility of controlling the outer-band transmission zeros in the presented filter. Fig. 10 shows the dependence of the transmissions zeros on the feeding angle (θ). As can be seen, both transmission zeros are controlled towards the same direction [23]. Referring also to Fig. 7, when θ decreases, M_{S1}/M_{SL} increases and M_{S2}/M_{SL} decreases resulting-in a decrease in the zeros' frequencies and vice versa. To locate both TZs closer to the passbands, the transferred energy through the nonresonating TM_{110} mode should increase with respect to the coupling of the resonating TM_{120}, TM_{210} modes [18]. A possible straight-forward option is by pushing the nonresonating TM_{110} mode to a higher frequency closer to the resonating TM_{120}, TM_{210} modes. This can be done at the first design steps with the selection of the DR and its dimensions.

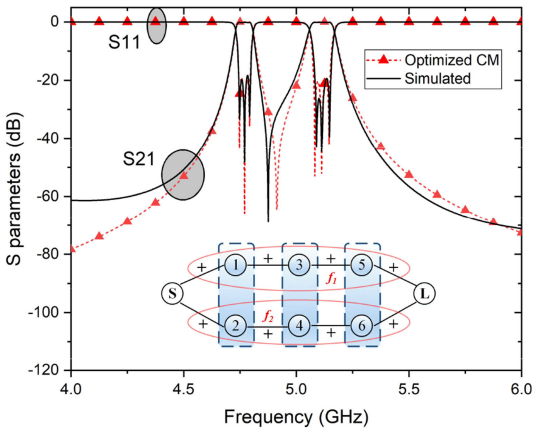

(a)

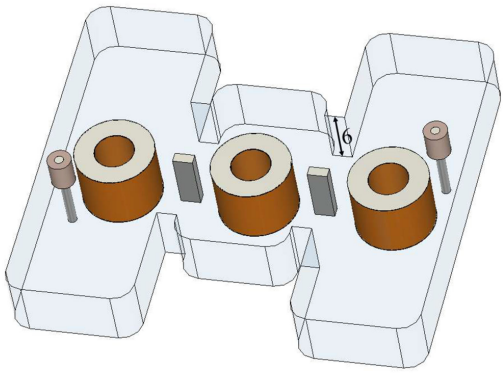

(b)

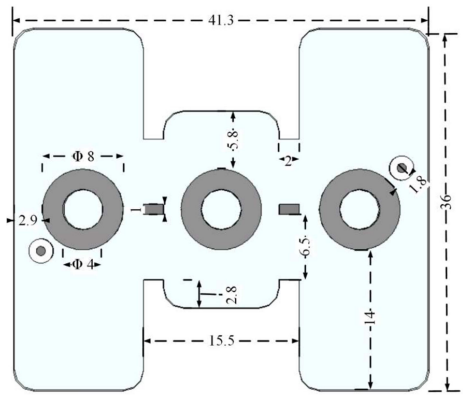

(c)

FIGURE 11. **Third-order dual-band dual-mode TM-mode DR filter in reversed IO configuration. (a) Coupling scheme, optimized coupling matrix (redline), and simulated S-parameters (blackline): with an inter-band transmission zero ($M_{5L} = M_{S1}$, $M_{6L} = M_{S2}$), and no outer-band transmission zero ($M_{SL} = 0$). (b) Perspective view. (c) Top view. All dimensions in mm unit.**

Another design example of a three-pole dual-band TM-mode DR filter is demonstrated in Fig. 11 to Fig. 14. The filter here is designed to operate at 4.77 GHz and 5.11 GHz with fractional bandwidths of 1.1% and 1.3%, respectively. The generalized corresponding coupling matrix is stated

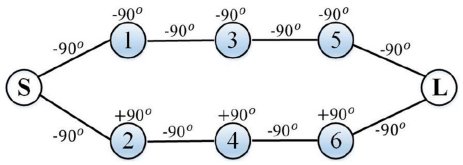

FIGURE 12. **Phase shift diagram of the presented 3rd-order dual-band filter in phase-reversed configuration (Fig. 11).**

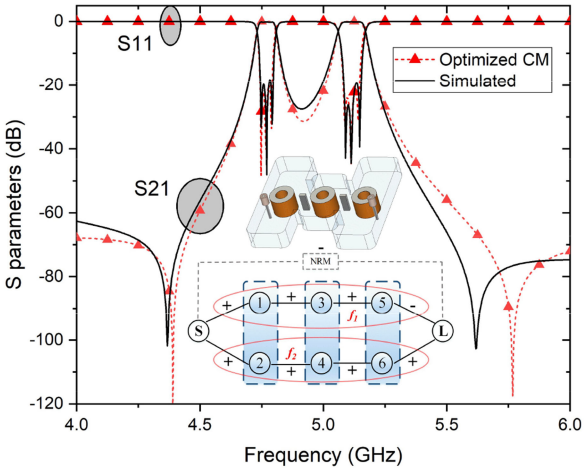

FIGURE 13. **3D structure, simulated S-parameters and optimized coupling matrix (CM) of the proposed third-order dual-band dual-mode TM-mode DR filter in aligned IO configuration. No inter-band transmission zero ($M_{5L} = -M_{S1}$, $M_{6L} = M_{S2}$). Outer-band transmission zeros are introduced ($M_{SL} < 0 = -0.00021$).**

in (7).

$$\begin{bmatrix} & S & 1 & 3 & 5 & 2 & 4 & 6 & L \\ S & 0 & 1.08 & 0 & 0 & 1.25 & 0 & 0 & 0 \\ 1 & 1.08 & 7.0 & 1.03 & 0 & 0 & 0 & 0 & 0 \\ 3 & 0 & 1.03 & 6.87 & 1.03 & 0 & 0 & 0 & 0 \\ 5 & 0 & 0 & 1.03 & 7.0 & 0 & 0 & 0 & 1.08 \\ 2 & 1.25 & 0 & 0 & 0 & -6.5 & 1.37 & 0 & 0 \\ 4 & 0 & 0 & 0 & 0 & 1.37 & -6.37 & 1.37 & 0 \\ 6 & 0 & 0 & 0 & 0 & 0 & 1.37 & -6.5 & 1.25 \\ L & 0 & 0 & 0 & 1.08 & 0 & 0 & 1.25 & 0 \end{bmatrix} \quad (7)$$

Structures and corresponding responses of the phase-reversed and in-phase configurations are demonstrated in Fig. 11 and Fig. 13, respectively. Here in these designs, the cavity length/width ratio is set larger than in the previous two-pole examples to obtain wider spacing between the two passbands (350 MHz). The simulated unloaded-Q for the lower passband is 3200, while in the upper passband is 3000. Similar to the two-pole designs, inter-band and outer-band TZs can be positioned effectively by controlling the I/O orientation. Fig. 11 depicts one configuration of the proposed third-order dual-band filter with an inter-band transmission zero having a high isolation level >70 dB. As discussed earlier, the appearance of this TZ is due to the phase reversal between the

TABLE 2. Total Phase Shifts for the Two Paths of the Three-Pole Dual-Band Filters

Filter		Phase shift at the transmission zero's frequency
1st filter with inter-band TZ	Lower passband (Resonators 1, 3, 5)	90° -90° -90° -90° -90° -90° -90° -90° $=-270^\circ$
	Upper passband (Resonators 2, 4, 6)	-90° $+90^\circ$ -90° $+90^\circ$ -90° $+90^\circ$ -90° -90° $=-90^\circ$
	Result	Out-of-phase
2nd filter with no inter-band TZ	Lower passband (Resonators 1, 3, 5)	-90° -90° -90° -90° -90° -90° -90° $+90^\circ$ $=-90^\circ$
	Upper passband (Resonators 2, 4, 6)	-90° $+90^\circ$ -90° $+90^\circ$ -90° $+90^\circ$ -90° -90° $=-90^\circ$
	Result	In-phase

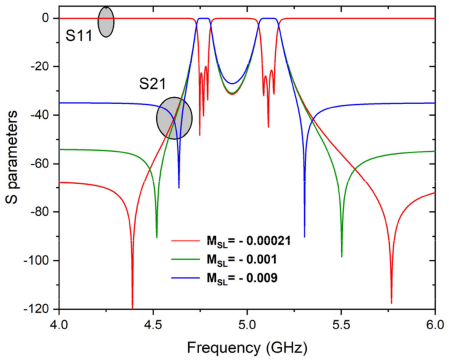

FIGURE 14. Optimized coupling matrix (CM) of the proposed thrid-order dual-band dual-mode TM-mode DR filter in aligned IO configuration with different S-L couplings.

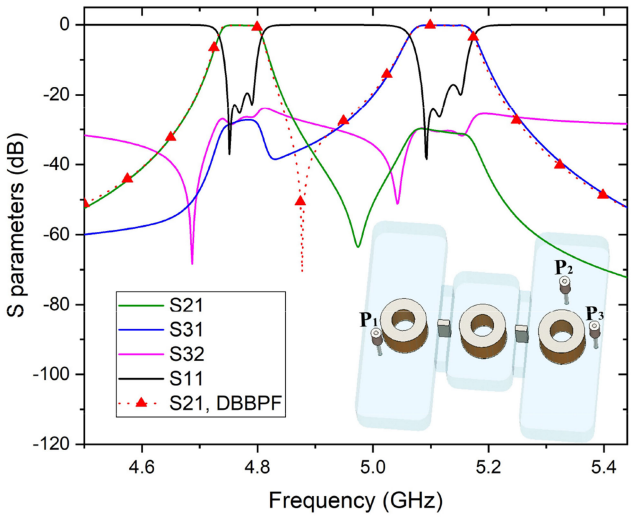

FIGURE 15. 3D structure and simulated S-parameters of a highly-miniaturized 3-pole diplexer using the proposed planar dual-mode TM-mode DR configuration. The structure dimensions and channels specifications are the same as the presented three-pole dual-band BPF examples. Input port (P_1) excites both orthogonal modes TM_{120},TM_{210}. Unlike the dual-mode configurations, each degenerate mode is excited separately at the output side. Port 2 (P_2) excites only TM_{120} mode constructing the RX channel. Port 3 (P_3) excites only TM_{210} mode forming the TX channel.

two paths of the filter as can be seen from the phase shift diagram in Fig. 12 and Table 2. Since each cavity causes a 180° phase shift to the signals ($3 \times 180^\circ$), the output probe is rotated 90° to keep the sign of M_{5L} positive. Consequently, the NRM bypass coupling is not excited and no outer-band TZs are obtained ($M_{SL} = 0$). The case is the opposite in the second dual-band filter example shown in Fig. 13. When the input and output ports are aligned, the sign of M_{5L} changes to negative and both signals become in-phase. As a result, the inter-band transmission zero cannot be introduced. On the other hand, the NRM bypass coupling is excited and creates two asymmetrical TZs at both edges ($M_{SL} < 0 = -0.00021$). Conceptually, the source-load coupling strength can be changed to control the positions of the TZs as can be seen in Fig. 14. Here, good isolation > 30 dB is obtained between the two passbands but with no inter-band TZ.

It should be noted that the design procedure and control process of the TZs of the presented 2nd and 3rd order filters extend and apply the same to all other multiples of even and odd cavities. Also, the proposed planar configuration can be utilized effectively to implement other miniaturized TM-mode DR components (e.g., diplexers, tunable filters). For example, a 3-pole ultra-compact TM-mode diplexer can be introduced by just modifying the output feeding mechanism of the proposed 3-pole dual-band dual-mode DR filter. All dimensions and passbands' specifications are the same as the dual-band filter. The only adjustment needed here is to modify the output structure to receive each channel separately unlike in the dual-band configuration. This can be done easily since the TM_{120}, TM_{210} modes are orthogonally distributed. Then, as shown in Fig. 15, the input probe (port 1) is positioned with 45° angle to excite both modes. On the other side, port 2 is positioned at an angle (θ=0°) to only excite the TM_{120} mode and receive only one channel corresponding to the lower passband of the dual-band filter. Similarly, port 3 is positioned orthogonally at 90° angle to only excite the TM_{210} mode and receive just the upper channel of the dual-band filter. As can be seen in Fig. 15, the passbands' specifications of the ultra-compact diplexer are ideally identical to the dual-band channels.

III. EXPERIMENTAL RESULTS AND COMPARISON

A three-pole C-band dual-band TM-mode dielectric resonator filter is manufactured and measured to validate the concept of the proposed planar configuration. A photograph of the implemented filter is shown in Fig. 16. The TM-mode dielectric resonator that has been used is an E6045 ($\varepsilon_r = 45$, $Q_u = 8000$ @ 5 GHz) from EXXELIA [24] with the same dimensions stated in the above section. The TM-mode dielectric resonators are then soldered in a compact metallic housing milled out of copper. Fig. 17 and Fig. 18 depict the measured responses of both the in-phase and phase-reversed configurations. Measurement results generally agree with simulations in the bandwidth specifications and the transmission zeros that have been created and controlled. A shift in the passband frequencies from simulated ones is noticed mainly due to the tuning process and uncertainty of the dielectric constant of

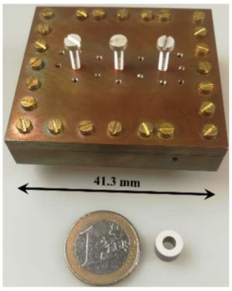

FIGURE 16. Photograph of the manufactured 3-pole dual-band dual-mode TM-mode DR filter. The used TM mode dielectric resonator and some of the tuning screws are also included.

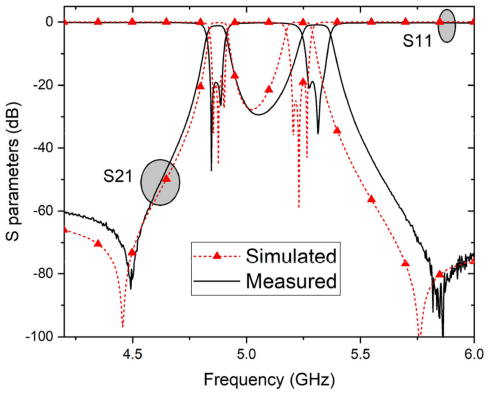

FIGURE 17. Simulated and measured S parameters of the implemented 3-pole dual-band dual-mode TM-mode DR filter in aligned IO configuration.

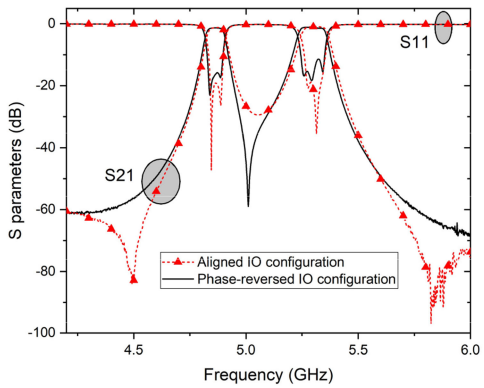

FIGURE 18. Measured results of the manufactured 3-pole dual-band dual-mode TM-mode DR filter in both aligned and phase-reversed IO configurations.

the DRs (100 MHz in the first passband, and 190 MHz in the upper band). The frequencies in simulations were then re-optimized to resemble the measured results. Fig. 17 shows the measured S parameter responses in comparison with the optimized simulations. The first passband operates at a centre frequency of 4.86 GHz with a 53.5 MHz of bandwidth compared to a bandwidth of 53.8 MHz in the simulated one (both at 15 dB level of S_{11}). The measured insertion loss is $\leq$1.1 dB and the return loss is better than 19 dB. The upper band has a

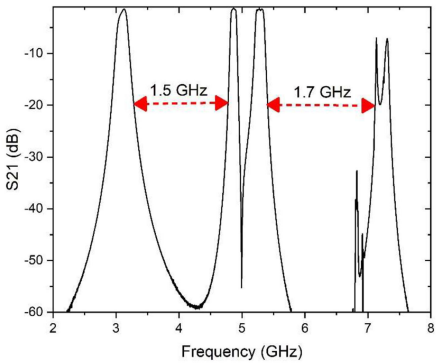

FIGURE 19. Wideband response of the presented 3-pole dual-band dual-mode TM-mode DR filter.

TABLE 3. Comparison With Other Reported Dual-Band Filters

Ref.	Technology	f_1 / f_2 (GHz)	FBW (%)	IL (dB)	Spurious-free band (GHz)	Controllable TZs
[5]	FWG	3.4/3.6	1.77/1.67	0.15/0.22	0.18	No
[10]	CDR	2.6/3.5	0.7/1.1	0.45/0.4	0.5	No
[11]	T-TMDR	4.25/4.55	1.5/1.5	1.3/1.15	NA	No
T.W.	P-TMDR	4.86/5.3	1.1/1.46	1.1/0.9	$\geq$1.5	Yes

T.W.: this work, FWG: folded waveguide, CDR: customized dielectric resonator, T-TMDR: transversal-TM mode dielectric resonator, P-TMDR: planar-TM mode dielectric resonator.

central frequency of 5.3 GHz with 77.2 MHz BW compared to 78.2 MHz of the simulated one. The mid-band insertion loss is lower than 0.9 dB and the return loss is better than 17 dB. Measurements and simulations have a good agreement in the lower passband frequency, while the measured higher passband has a slight shift of 50 MHz from simulations. This could be due to the sensitivity of this band (TM_{210}) to the central post as aforementioned, especially since the resonators are positioned very close to the central post and the cavity. Fig. 18 depicts the measurements of the implemented filter in both in-phase and out-of-phase configurations obtained by the rotation of the output probe. As can be seen, an inter-band TZ provides high isolation between the two passbands up to 60 dB in the out-of-phase case, while two outer-band TZs are introduced in the in-phase configuration. Silver-plated tuning screws (shown or located where the empty holes in Fig. 16) were added similar to those in Fig. 4(b) to tune both frequencies or each one independently, inter-resonator couplings, and the IO couplings. The extracted unloaded Q factor is better than 1040 ($\approx$ 35% of the simulated ones). Silver-plating and larger dielectric resonators can be considered to increase the Q_u up to 3000. The filter has a compact size of 41.3 $\times$ 36 $\times$ 5.9 mm^3 offering more than 70% volume reduction than the conventional waveguide structure. Fig. 19 exhibits the measured wideband response of the implemented filter. As shown, the filter has a good spurious-free band of 1.5 GHz at the lower side, 1.7 GHz to the next higher unwanted spurious frequency. Table 3 summarizes a comparison between the proposed compact inline dual-band dual-mode TM mode BPF and similar designs. The filter has a good spurious-free band

≥1.5 GHz which is better than the other configurations. Also, the proposed filter offers the advantage of effective introduction and control of inter-band and outer-band transmission zeros. Despite that the transversal configuration in [11] is able to introduce multiple inter-band and outer-band TZs, those TZs are sensitive to many parameters and cannot be effectively controlled. Contrary, the generated inter-band TZ in the proposed planar configuration is controlled just through the phase shift between the two signal paths and it is not affected by any other parameters. Additionally, whereas the structure must be folded in [5] to introduce both inter-band and outer-band TZs at both sides, out-of-band rejection characteristics of the inline filters in [10] and [11] need to be improved either at one or both edges. While the presented configuration has shown the capability of obtaining and controlling inter-band and outer-band TZs at both edges to provide higher out-of-band rejections. Nevertheless, it should be mentioned that the positioning of the outer-band TZs closer to the passband is not easy and the coupling ratio of the nonresonating TM_{110} mode should be considered carefully. Another attractive advantage of the proposed planar topology is that it makes the assembly and tuning process easier and more feasible than the transversal configurations resulting-in better responses and less implementation effort. Post-tuning is even more important in such designs where each of the two signals needs to properly couple and excited in the same single cavity with the same IO feedings. Advantageously, the introduced planar configuration allows the designer to introduce tuning screws to efficiently control all resonant frequencies, bandwidths, and IO couplings.

IV. CONCLUSION

A miniaturized dual-band dual-mode TM-mode dielectric filter is presented in planar configuration for the first time. The use of the TM-mode DRs and the orthogonal degenerate TM_{120} and TM_{210} modes effectively provide substantial compactness with high Q_u and good spurious-free response. Also, high inter-band isolation and outer-band rejections are obtained through the introduction of flexibly controlled transmission zeros. The proposed planar configuration brings various advantages in comparison with the transversal configuration including easier tuning, assembly, and production. All these features strongly promote the employment of the presented planar design in other ultra-compact components (e.g., tunable filters, diplexers). A prototype has been manufactured and the measurements allow for the design approach to be verified.

REFERENCES

[1] R. V. Snyder, A. Mortazawi, I. Hunter, S. Bastioli, G. Macchiarella, and K. Wu, "Present and future trends in filters and multiplexers," *IEEE Trans. Microw. Theory Techn.*, vol. 63, no. 10, pp. 3324–3360, Oct. 2015, doi: 10.1109/TMTT.2015.2475245.

[2] A. Widaa, C. J. You, and M. Awad, "Compact single/dual-band bandpass filters with independently controllable passbands using staircase resonators," in *Proc. Int. Conf. Comp. Control Elect. Elec. Eng.*, 2021, pp. 1–4, doi: 10.1109/ICCCEEE49695.2021.9429611.

[3] Y. Zhu and Y. Dong, "A compact dual-band quasi-elliptic filter based on hybrid SIW and microstrip technologies," *IEEE Trans. Circuits Syst. II, Exp. Briefs*, vol. 69, no. 3, pp. 719–723, Mar. 2022, doi: 10.1109/TCSII.2021.3111860.

[4] S. Amari and M. Bekheit, "A new class of dual-mode dual-band waveguide filters," *IEEE Trans. Microw. Theory Techn.*, vol. 56, no. 8, pp. 1938–1944, Aug. 2008, doi: 10.1109/TMTT.2008.927411.

[5] L. Zhu, R. R. Mansour, and M. Yu, "Quasi-elliptic waveguide dual-band bandpass filters," *IEEE Trans. Microw. Theory Techn.*, vol. 67, no. 12, pp. 5029–5037, Dec. 2019, doi: 10.1109/TMTT.2019.2948856.

[6] L. Zhu, R. R. Mansour, and M. Yu, "Compact waveguide Dual-band filters and diplexers," *IEEE Trans. Microw. Theory Techn.*, vol. 65, no. 5, pp. 1525–1533, May 2017, doi: 10.1109/TMTT.2016.2642957.

[7] J. A. Ruiz-Cruz, M. M. Fahmi, and R. R. Mansour, "Triple-conductor combline resonators for dual-band filters with enhanced guard-band selectivity," *IEEE Trans. Microw. Theory Techn.*, vol. 60, no. 12, pp. 3969–3979, Dec. 2012, doi: 10.1109/TMTT.2012.2223482.

[8] E. Doumanis, L. Guan, G. Goussetis, and D. Ferling, "Dual-band bandpass double ground plane coaxial resonators and filters," *IEEE Trans. Microw. Theory Techn.*, vol. 66, no. 8, pp. 3828–3835, Aug. 2018, doi: 10.1109/TMTT.2018.2841838.

[9] Y. Xie and F. -C. Chen, "Dual-band and wide stopband coaxial filters using open-circuited-stub-loaded resonators," *IEEE Trans. Circuits Syst. II, Exp. Briefs*, vol. 68, no. 6, pp. 1872–1876, Jun. 2021, doi: 10.1109/TCSII.2020.3044372.

[10] R. Zhang and R. R. Mansour, "Dual-band dielectric-resonator filters," *IEEE Trans. Microw. Theory Techn.*, vol. 57, no. 7, pp. 1760–1766, Jul. 2009, doi: 10.1109/TMTT.2009.2022876.

[11] V. Nocella, L. Pelliccia, C. Tomassoni, and R. Sorrentino, "Miniaturized dual-band waveguide filter using TM dielectric-loaded dual-mode cavities," *IEEE Microw. Wireless Compon. Lett.*, vol. 26, no. 5, pp. 310–312, May 2016, doi: 10.1109/LMWC.2016.2549181.

[12] J. Chen, J. Li, and J. Shi, "Miniaturized dual-band differential filter using dual-mode dielectric resonator," *IEEE Microw. Wireless Compon. Lett.*, vol. 28, no. 8, pp. 657–659, Aug. 2018, doi: 10.1109/LMWC.2018.2842681.

[13] M. Höft, "Bandpass filter using TM-mode dielectric rod resonators with novel input coupling," in *IEEE MTT-S Int. Microw. Symp. Dig.*, 2009, pp. 1601–1604, doi: 10.1109/MWSYM.2009.5166018.

[14] S. Amari and U. Rosenberg, "A universal building block for advanced modular design of microwave filters," *IEEE Microw. Wireless Compon. Lett.*, vol. 13, no. 12, pp. 541–543, Dec. 2003, doi: 10.1109/LMWC.2003.820637.

[15] S. Amari and M. Bekheit, "New dual-mode dielectric resonator filters," *IEEE Microw. Wireless Compon. Lett.*, vol. 15, no. 3, pp. 162–164, Mar. 2005, doi: 10.1109/LMWC.2005.844210.

[16] H. Hu and K. Wu, "A TM11 dual-mode dielectric resonator filter with planar coupling configuration," *IEEE Trans. Microw. Theory Techn.*, vol. 61, no. 1, pp. 131–138, Jan. 2013, doi: 10.1109/TMTT.2012.2226741.

[17] A. Widaa, C. Bartlett, and M. Höft, "Miniaturized all-reconfigurable dual-mode dielectric filter using piezomotors for future satellite communications," in *Proc. 51th Eur. Microw. Conf.*, London, U.K., 2022.

[18] S. Bastioli and R. V. Snyder, "Nonresonating modes do it better!: Exploiting additional modes in conjunction with operating modes to design better quality filters," *IEEE Microw. Mag.*, vol. 22, no. 1, pp. 20–45, Jan. 2021, doi: 10.1109/MMM.2020.3027934.

[19] L. Zhu, "High-Q multi-band filters," Ph.D. dissertation, Dept. Elec. Comput. Eng., Univ. Waterloo, Canada, 2019.

[20] R. J. Cameron, C. M. Kudsia, and R. R. Mansour, *Microwave Filters for Communication Systems: Fundamentals, Design, and Applications*, 2nd ed. Hoboken, NJ, USA: Wiley, 2018, doi: 10.1002/9781119292371.

[21] J. B. Thomas, "Cross-coupling in coaxial cavity filters – A tutorial overview," *IEEE Trans. Microw. Theory Techn.*, vol. 51, no. 4, pp. 1368–1376, Apr. 2003, doi: 10.1109/TMTT.2003.809180.

[22] L. Zhu, R. R. Mansour, and M. Yu, "Triple-band cavity bandpass filters," *IEEE Trans. Microw. Theory Techn.*, vol. 66, no. 9, pp. 4057–4069, Sep. 2018, doi: 10.1109/TMTT.2018.2846725.

[23] C. Tomassoni, S. Bastioli, and R. Sorrentino, "Generalized TM dual-mode cavity filters," *IEEE Trans. Microw. Theory Techn.*, vol. 59, no. 12, pp. 3338–3346, Dec. 2011, doi: 10.1109/TMTT.2011.2172622.

[24] EXXELIA, 2015. Accessed: Jan. 20, 2022. [Online]. Available: https://exxelia.com/uploads/PDF/e7000-v1.pdf

ABDULRAHMAN WIDAA (Graduate Student Member, IEEE) was born in Wad Medani, Gezira, Sudan, in 1991. He received the B.Sc. degree (Hons.) in telecommunication engineering from the University of Gezira, Wad Madani, Sudan, in 2014, and the M.Eng. degree in telecommunication engineering from the University of Electronic Science and Technology of China, Chengdu, China, in 2018. He is currently working toward the Dr.-Ing. degree in electrical and information engineering with Kiel University, Kiel, Germany. From 2014 to 2016, he was a Teaching Assistant with the Electronics Engineering Department, University of Gezira. From 2016 to 2018, he was a Research Assistant with the University of Electronic Science and Technology of China, where he was involved in the design of tunable filters for RF/microwave applications. From 2018 to 2019, he was a Lecturer with the Electronics Engineering Department, University of Gezira. Since 2019, he has been an EU-Researcher with the Chair of Microwave Engineering, Kiel University, under EU Project of Advanced Technologies for future European Satellite Applications (TESLA). He was a Visiting Researcher with Technische Universität Darmstadt, Darmstadt, Germany during February–March 2020, University of Perugia, Perugia, Italy, and RF Microtech S.r.l, Italy during May–July 2021. His research interests include the design of miniaturized/tunable filters and components for microwave and satellite communications, sensors, and embedded systems. He was the recipient of many national and international awards, scholarships, and grants including the Chinese University Master Scholarship Program in 2016 and European Microwave Week Student Grant in 2020 and 2021, respectively.

MICHAEL HÖFT (Senior Member, IEEE) received the Dipl.-Ing. degree in electrical engineering and the Dr.-Ing. degree from Hamburg University of Technology, Hamburg, Germany, in 1997 and 2002, respectively. From 2002 to 2013, he was with the Communications Laboratory, European Technology Center, Panasonic Industrial Devices Europe GmbH, Lüneburg, Germany. He was a Research Engineer and the Team Leader, where he was involved in the research and development of microwave circuitry and components, particularly filters for cellular radio communications. From 2010 to 2013, he was the Group Leader of the research and development of sensor and network devices. Since 2013, he has been a Full Professor with the Faculty of Engineering, Kiel University, Kiel, Germany, where he is currently the Head of the Chair of Microwave Engineering, Institute of Electrical and Information Engineering. His research interests include active and passive microwave components, sub-millimeter-wave quasi-optical techniques and circuitry, microwave and field measurement techniques, microwave filters, microwave sensors, and magnetic field sensors. Dr. Höft is a member of the European Microwave Association, the Association of German Engineers, and the German Institute of Electrical Engineers.